

Investigating turbulence in wind flow over complex terrain

By J. P. O'Sullivan[†], R. Pecnik AND G. Iaccarino

Increasing worldwide wind energy production means wind farms are being constructed in areas where the terrain is more complex. Two important features of wind flow over complex terrain are flow separation and anisotropic turbulence. The most commonly used simulation approaches for wind flow use the Reynolds-averaged Navier-Stokes (RANS) equations with a $k - \varepsilon$ turbulence closure. A model using this closure has difficulty in estimating separation accurately and cannot represent turbulent anisotropy. In other applications the v^2f turbulence closure has shown good ability to predict flow separation. Similarly, the algebraic structure-based turbulence model (ASBM) has shown promise in capturing turbulent anisotropy. In the present study the flow over a representative hill that includes these features is calculated using the RANS equations with both the v^2f and ASBM closures. A novel implementation of the ASBM closure is developed allowing a stable, smooth solution to be obtained. The results are compared with experimental data for the same flow, and a good agreement is obtained for the separated region and the Reynolds stress components. Wall functions are developed for the v^2f closure to enable the simulation of higher Reynolds number flows both with and without surface roughness. The results are compared with experimental data and are shown to accurately capture the separated region.

1. Introduction

The study of wind flow in the atmospheric boundary layer (ABL) is important in many applications. The dispersion of pollutants and hazardous materials, wind loading on man-made structures, and prediction of local weather conditions are just a few examples. One of the most significant applications at present is the production of energy from wind. As the world struggles to come to terms with the issues of climate change and the rising cost of fossil fuels, renewable energy has become the focus of much public, political, and scientific interest. Wind farms, once installed, have the potential to provide clean, inexhaustible energy resources that can generate enough electricity to power millions of homes and businesses. The World Wind Energy Association reports that by the end of 2008, 120 Gigawatts of wind power capacity were installed worldwide. This represents more than 1.5% of global electricity consumption and is an increase of 26 Gigawatts since the end of 2007.

Early wind farms tended to be constructed in areas where the terrain is relatively smooth and simple. Now, as a result of this trend of increasing the worldwide wind energy production, wind farms are being constructed in areas where the terrain is more complex. This is especially true of New Zealand where almost all available terrain is complex. More complex terrain means that predicting important parameters, such as power production, turbine fatigue life, and peak velocities, is much more complicated and requires the use of more sophisticated computational fluid dynamics (CFD) tools.

[†] University of Auckland, Auckland, New Zealand

For many years the computational method used most commonly for modelling wind flow has been the wind atlas methodology (Landberg *et al.* 2003). In simple terms, this method uses linearized flow equations to correct existing long-term measurements for several different effects including sheltering objects, terrain classification, and domain contours. The advantage of this method is that its well established and simple to use. By far the most widely used application of this method is the WAsP computer code developed by the RISØ National Laboratory in Denmark.

WAsP has enjoyed such widespread success because the use of linearized flow equations make it able to predict the wind resource accurately and efficiently when the terrain is sufficiently smooth to ensure attached flows. However, as Bowen & Mortensen (1996) pointed out, WAsP was increasingly being used to predict wind flow over sites that had sufficiently complex terrain as to no longer fall within the operational envelope of the software. In an attempt to quantify the problem, a site ruggedness index (RIX) was proposed as a coarse measure of the terrain complexity and hence the extent of flow separation. The RIX is defined as “the fractional extent of the surrounding terrain which is steeper than a certain critical slope” (Mortensen *et al.* 2006). Upon revisiting the issue ten years later, despite corrections using the RIX, Mortensen *et al.* (2006) still conclude that it is not in general advisable to apply WAsP in complex terrain. This conclusion has been reached by many researchers (Landberg *et al.* 2003; Palma *et al.* 2008; Perivolaris *et al.* 2006; Wood 2000). When these conclusions are combined with the observation that the increase in wind power production has led to sites being selected with more complex terrain (Palma *et al.* 2008), it is clear that alternative computational methods must be found.

CFD is the obvious choice as an alternative to WAsP and other linearized approaches, with the RANS approach the most likely choice given the computational constraints. However, Palma *et al.* (2008) note that despite their impact in many areas, such as the automotive or aeronautical engineering, CFD techniques have not yet become common in wind energy engineering. Hargreaves & Wright (2007) observe that while CFD packages are now widely used by wind engineers, they are not suitable for ABL flows using their standard settings. In particular, using the standard $k - \varepsilon$ model for the turbulence closure is not sufficient for capturing the important dynamics of wind flow over complex terrain. Undheim *et al.* (2006) note that turbulence modelling is still a major challenge, particularly in complex terrain, and that more accurate turbulence models are required for atmospheric flow. Both Eidsvik (2005) and Hanjalic (2005) observe that the inability of the standard turbulence models to accurately reproduce the anisotropy of turbulence leads to limitations in many applications of wind flow modelling. Hanjalic (2005) goes on to state that the “limitations of linear eddy viscosity models (EVMs) have been recognized already in the early days of turbulence modeling and the attention has been turned to the second moment closure (SMC) that makes the most logical and physically most appropriate RANS modeling framework”. Eidsvik (2005) supports this idea saying that stratified flows over hills may also contain domains with mean velocity maxima and adverse pressure gradients suggesting that full dynamic modelling of the Reynolds stress components may be desirable.

In their work for the 2008 CTR Summer Program, Radhakrishnan *et al.* (2008) note that whereas eddy viscosity models are not accurate in predicting complex flows, Reynolds Stress models are difficult to implement numerically and tend to have high computational stiffness. Instead they adopt an approach using the algebraic structure-based turbulence model (ASBM). This is based on the eddy-axis concept (Kassinos & Reynolds 1994)

which is used to relate the Reynolds stress and structure tensors to parameters of a hypothetical turbulent eddy field. Each eddy represents a two-dimensional turbulence field and is characterized by an eddy-axis vector. The turbulent motion associated with this eddy is decomposed into a component along the eddy axis, the jetal component, and a component perpendicular to the eddy axis, the vortical component. This motion can be further allowed to be flattened in a direction normal to the eddy axis (a round eddy being characterized by a random distribution of kinetic energy around its axis). Averaging over an ensemble of turbulent eddies gives statistical quantities representative of the eddy field, along with an algebraic constitutive equation for the normalized Reynolds stresses, R_{ij} . This algebraic equation relates the Reynolds stress tensor to the mean strain rate and rotation rate tensors, an eddy flattening parameter, a projection tensor for wall-blocking and two turbulent scales. Partial differential equations are solved for the turbulent scales, while the blocking parameter is obtained through an elliptic relaxation procedure. A history of the development of the ASBM model is given along with a detailed description of its implementation by Radhakrishnan *et al.* (2008). Their results compared well with previously published experimental and direct numerical simulation (DNS) results for both a backwards facing step and an axisymmetric diffuser. This demonstrates the ability of the ASBM model to accurately predict the dynamics of separated flow, which is an important criterion for modelling wind flow in complex terrain.

The first objective of this project was to investigate the ability of the ASBM closure, as implemented by Radhakrishnan *et al.* (2008), to predict a two-dimensional, steady-state flow over a representative Saussian ridge. This was a direct extension of their work, but by investigating a different, more representative geometry it provided an insight into the usefulness of the closure in modelling wind flow. Results were obtained for both the v^2f and the ASBM closures, and comparisons were made with the experimental data set of Loureiro *et al.* (2007).

The second objective was to develop a wall function approach for the v^2f closure. Currently CFD simulations of the ABL require the use of wall functions to specify the boundary condition at the ground. As Loureiro & Silva Freire (2009) note, although low Reynolds number turbulence models provide an alternative, their requirement that the grid be very finely resolved at the wall makes them impractical for many environmental and industrial flow simulations. In their work Radhakrishnan *et al.* (2008) used a grid that is compressed vertically to ensure that $y^+ < 1.0$. In the present research the same resolution was used in the initial simulations; however, the developed wall functions also allowed the use of much coarser grids. The wall functions also enabled the inclusion of roughness in the model of the ground interaction, and comparisons were made between the results obtained and the experimental data set of Loureiro *et al.* (2009).

2. Preliminaries

2.1. Formulation

The steady state RANS equations that govern the motion of wind flow are

$$\bar{U}_j \frac{\partial \bar{U}_i}{\partial x_j} = -\frac{1}{\rho} \frac{\partial \bar{p}}{\partial x_i} + \frac{\partial}{\partial x_j} \left(\nu \frac{\partial \bar{U}_i}{\partial x_j} \right) - \frac{\partial \langle u'_i u'_j \rangle}{\partial x_j} \quad (2.1)$$

$$\frac{\partial \bar{U}_i}{\partial x_i} = 0, \quad (2.2)$$

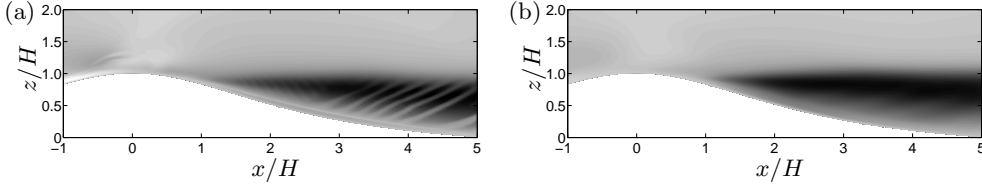


FIGURE 1. Solution for ASBM closure with (a) original algorithm and (b) new coupling.

where \bar{U}_i are the components of the mean velocity, \bar{p} the mean pressure, and $\langle u'_i u'_j \rangle$ the components of the Reynolds stress tensor. For many turbulence closures, including the $k - \varepsilon$ and the $v^2 f$ closures, the Boussinesq approximation is used to relate the Reynolds stress tensor to an eddy viscosity ν_T and the strain rate tensor S_{ij} :

$$-\langle u'_i u'_j \rangle = 2\nu_T S_{ij} - \frac{2}{3}k\delta_{ij}. \quad (2.3)$$

Substituting Eq. (2.3) into the momentum equations (2.1), the RANS equations become

$$\bar{U}_j \frac{\partial \bar{U}_i}{\partial x_j} - \frac{\partial}{\partial x_j} \left[(\nu + \nu_T) \frac{\partial \bar{U}_i}{\partial x_j} \right] = -\frac{\partial \hat{p}}{\partial x_i} + \frac{\partial}{\partial x_j} \left(\nu_T \frac{\partial \bar{U}_j}{\partial x_i} \right), \quad (2.4)$$

where \hat{p} is the modified mean pressure which has absorbed the density and the hydrostatic part of the turbulent kinetic energy. Note that for an incompressible RANS solver based on a standard SIMPLE algorithm, the terms on the left-hand side of Eq. (2.4), including the diffusion term with the eddy viscosity, are treated implicitly. This is a straightforward procedure when the Reynolds stresses are approximated with the Boussinesq assumption.

In contrast, the ASBM closure calculates the components of the Reynolds stresses $\langle u'_i u'_j \rangle$ directly without the use of the Boussinesq approximation. In order to maintain a stable algorithm, the eddy viscosity is kept on the left-hand side and subtracted explicitly on the right-hand side following a so-called deferred-correction approach, Kalitzin *et al.* (2004). This approach can be written as

$$\bar{U}_j^{(n)} \frac{\partial \bar{U}_i^{(n+1)}}{\partial x_j} - \frac{\partial}{\partial x_j} \left[(\nu + \nu_T)^{(n)} \frac{\partial \bar{U}_i^{(n+1)}}{\partial x_j} \right] = -\frac{\partial \hat{p}}{\partial x_i} - \frac{\partial \langle u'_i u'_j \rangle}{\partial x_j} - \frac{\partial}{\partial x_j} \left(\nu_T \frac{\partial \bar{U}_i}{\partial x_j} \right) \Big|^{(n)}, \quad (2.5)$$

with n and $n + 1$ indicating the previous and the new time step, respectively. Once a converged solution is obtained, the terms involving the eddy viscosity cancel out leaving only the ASBM Reynolds stress components. The eddy viscosity is calculated by the turbulence closure used, in this case the $v^2 f$ model.

Although using this explicit correction enables the implementation of a stable algorithm for the ASBM closure, the highly nonlinear nature of the closure means that obtaining a smooth, converged steady state solution is often difficult (see spurious streaks of $\langle u'u' \rangle$ behind hill in Fig. 1, left). In order to obtain converged solutions without these oscillations, a new coupling method is proposed by introducing a blending between the Boussinesq and ASBM stresses as follows:

$$\begin{aligned} \bar{U}_j^{(n)} \frac{\partial \bar{U}_i^{(n+1)}}{\partial x_j} - \frac{\partial}{\partial x_j} \left[(\nu + \nu_T)^{(n)} \frac{\partial \bar{U}_i^{(n+1)}}{\partial x_j} \right] &= -\frac{\partial \hat{p}}{\partial x_i} \\ &+ \frac{\partial}{\partial x_j} \left[(1 - \alpha) \nu_T \frac{\partial \bar{U}_j}{\partial x_i} - \alpha \left(\nu_T \frac{\partial \bar{U}_i}{\partial x_j} + \left(\langle \widetilde{u'_i u'_j} \rangle - \frac{2}{3}k\delta_{ij} \right) \right) \right] \Big|^{(n)}. \end{aligned} \quad (2.6)$$

For $\alpha = 0$, Eq. (2.4) with the Boussinesq approximation is recovered, whereas for $\alpha = 1$ and the solution being converged (timestep $n + 1 \rightarrow n$), the Boussinesq approximation cancels out and only the ASBM stresses remain on the right-hand side. For the simulations presented herein α is set to 0.5 and gradually increased to $\alpha = 1$. Furthermore, the tilde over the ASBM Reynolds stress components indicates that these values have been filtered at each iteration. The filtering is done with a top hat filter based on the neighboring cells. Note that by subtracting the isotropic contribution from the ASBM Reynolds stress components, the definition of \hat{p} is consistent for all values of α . Figure 1 shows the improvement in the solution obtained using this new coupling method.

2.2. Wall Functions

Wall functions apply boundary conditions at some distance from the wall, which removes the requirement to solve the governing equations all the way to the wall. This has two important benefits in simulations of wind flow. First, it significantly reduces the computational resource required by allowing the use of a much coarser grid near the wall. Second, by applying the boundary conditions at some point away from the wall the exact geometry of the wall does not need to be fully resolved. This allows the complex geometries caused by terrain effects, vegetation, etc., to be modelled by including an equivalent roughness in the wall functions. The wall functions used in the present research are based on the standard wall-function model presented by Launder & Spalding (1974) and the rough wall model derived from it. It assumes that the mean flow is approximately parallel to the wall and thus log law relations can be applied as boundary conditions at the first cell center away from the wall. Also, the friction velocity is modelled using the turbulent kinetic energy in the near wall cell (Wilcox 1998):

$$u^* = C_\mu^{1/4} k_p^{1/2}, \quad (2.7)$$

where C_μ is a constant taken from the turbulence closure. This means that the non-dimensional wall distance y^+ can be approximated by

$$y^+ = \frac{C_\mu^{1/4} k_p^{1/2} y_p}{\nu}, \quad (2.8)$$

where y_p is the normal distance from the wall to the center of the first cell. Similarly, for smooth walls, the non-dimensional wall velocity U^+ is given by

$$U^+ = \frac{1}{\kappa} \ln(y^+) + B, \quad (2.9)$$

where κ is von Kármán's constant and B is the log law constant, which is equal to 5.2. The log law approximations are not applied directly to the velocity variables but instead are used to adjust the eddy-viscosity at the wall.

$$\nu_T = \nu \left(\frac{y^+}{U^+} - 1 \right). \quad (2.10)$$

Similarly, the turbulent kinetic energy is not defined by the wall function at the cell nearest to wall, but instead the wall shear stress is approximated using the log law and this is included in the production of term in the turbulent kinetic energy equation:

$$P_k = \tau_w \left. \frac{\partial u}{\partial y} \right|_p, \quad \text{with:} \quad \tau_w = C_\mu^{1/4} k_p^{1/2} \frac{\bar{U}_p}{U^+}, \quad (2.11)$$

where \bar{U}_p is the mean velocity tangential to the wall in the cell nearest to the wall. For the dissipation however, the value is defined directly by the wall function method:

$$\varepsilon_p = \frac{C_\mu^{3/4} k_p^{3/2}}{\kappa y_p}. \quad (2.12)$$

Finally, the effects of roughness are easily introduced into wall functions of this form by adjusting the non-dimensional wall velocity accordingly:

$$U_{rough}^+ = \frac{1}{\kappa} \ln \left(\frac{y^+}{K_s^+} \right) + B_{rough}, \quad (2.13)$$

where K_s^+ is the non-dimensional equivalent grain-of-sand roughness height, which is determined by the surface, and B_{rough} is the rough wall log law constant, which was set to 8.5 following Pope (2000). For the remaining variables, v^2 , f , and \hat{p} , the boundary conditions were applied at the wall in the same manner as the fully resolved simulations. It is important to note that a requirement for using the wall function boundary conditions is that the point of application must be inside the log law region. For fully turbulent flows this means that grids must be selected such that this point is at $y^+ = 30$ or greater.

3. Numerical Method

3.1. Solver details

The simulations in the present work were carried out using both Stanford's in-house code CDP and the open source CFD solver OpenFOAM. CDP is a vertex-based, unstructured, finite-volume solver that uses an implicit predictor-corrector approach to solve the incompressible RANS equations. OpenFOAM is a cell-centered, unstructured, finite-volume solver that also uses an approach based on the SIMPLE algorithm. Both solvers used the same FORTRAN library to calculate the explicit ASBM correction. The wall functions for the $v^2 f$ closure were implemented only in the CDP code.

3.2. Computational domain

The computational domain for all of the simulations was designed to be equivalent to the experimental set up used by Loureiro *et al.* (2007). For the entire domain the height was $4H$, and an inlet section of $7.5H$ was present before encountering the hill of height H . The hill itself was $10H$ wide and following it was a $10H$ outlet section. The shape of the hill was a modified "Witch of Agnesi" profile given by

$$z_H(x) = H_1 \left[1 + (x/L_H)^2 \right]^{-1} - H_2, \quad (3.1)$$

where $H_1 = 75\text{mm}$, $H_2 = 15\text{mm}$, $L_H = 150\text{mm}$, and $H = H_1 - H_2 = 60\text{mm}$. For the low Reynolds number simulations, a grid was used with 300 cells in the streamwise direction and 66 cells in the vertical direction. The cells in the streamwise direction were compressed in the region around the hill, and throughout the domain the cells were compressed in the vertical direction to ensure that $y^+ < 1.0$. For the high Reynolds number simulations with the rough wall functions, the grid was 300 cells in the streamwise direction and 52 cells in the vertical direction. Again the cells in the streamwise direction were compressed in the region around the hill, and throughout the domain the cells were compressed in the vertical direction but only such that $y^+ \approx 50$.

3.3. Boundary conditions

Profiles for \bar{U} , k , ε , and v^2 were applied at the inlet boundary for all of the simulations. Zero flux was prescribed for the remaining variables f , ϕ , and \hat{p} . The profiles were obtained from the converged v^2f solution of a boundary layer where the boundary layer height matched the experimental results at the inlet of the domain. An outlet boundary condition was used at the outlet, prescribing a reference value for \hat{p} and zero flux for all other variables. At the top of the domain zero flux was used for all variables as the boundary was sufficiently far away from the top of the hill. For the ground boundary conditions, no slip was used for the fully resolved simulations, and the wall functions described in section 2.2 were used for the coarse grids. To ensure that the wall function boundary conditions could accurately capture the flow details, a number of fully resolved simulations of channel flows were made. They were then compared with results from coarse grid simulations of the same channels using the wall functions. The agreement was found to be sufficiently good to give confidence in the application of the wall function boundary conditions.

4. Results and discussion

4.1. Low Re simulations

The low Reynolds number simulations were carried out so that the results could be compared with the experimental data from Loureiro *et al.* (2007). The boundary layer thickness for the incoming flow was 100mm and the Reynolds number 4,772. Figure 2 shows the results for the streamwise velocity and the Reynolds stress components using the ASBM closure. Note that for each plot in the figure the profiles are scaled by different amounts to increase their readability. Thus whereas each of the components of the Reynolds stresses appears similar throughout the domain, when the scaling is removed they are significantly different. This demonstrates the anisotropic nature of the Reynolds stresses in wall-bounded flows and emphasises the need for turbulence closures capable of representing them. For the mean streamwise velocity the agreement with the experimental results is very good. The separated region is captured accurately, including the point of reattachment. There is a slight under-estimation of its height around $x/H = 1.0$ and a slight over estimation around $x/H = 7.0$. The qualitative agreement for the Reynolds stresses is good throughout the domain. For all three stresses the form of the profiles is in good agreement but the magnitudes are underpredicted in and around the separated region. The most energy carrying stress, $\langle u'u' \rangle$, is the most accurately estimated, though even this is underpredicted at the start of the separated region.

Figure 3 shows a more detailed comparison of results for both the ASBM closure and the v^2f closure with the experimental data in the separated region. The results for mean velocities are in excellent agreement with the experimental data for both. However, it can be seen that although both closures agree well in the region immediately following separation, the ASBM closure estimates the height of the separation bubble more accurately farther downstream at $2.5H$ and $4H$. It is also anticipated that the difference between the two closures will be more pronounced in fully three-dimensional flows.

4.2. High Re simulations

In order to assess the effectiveness of the wall functions that had been developed for the v^2f closure, higher Reynolds number simulations were necessary. This is because

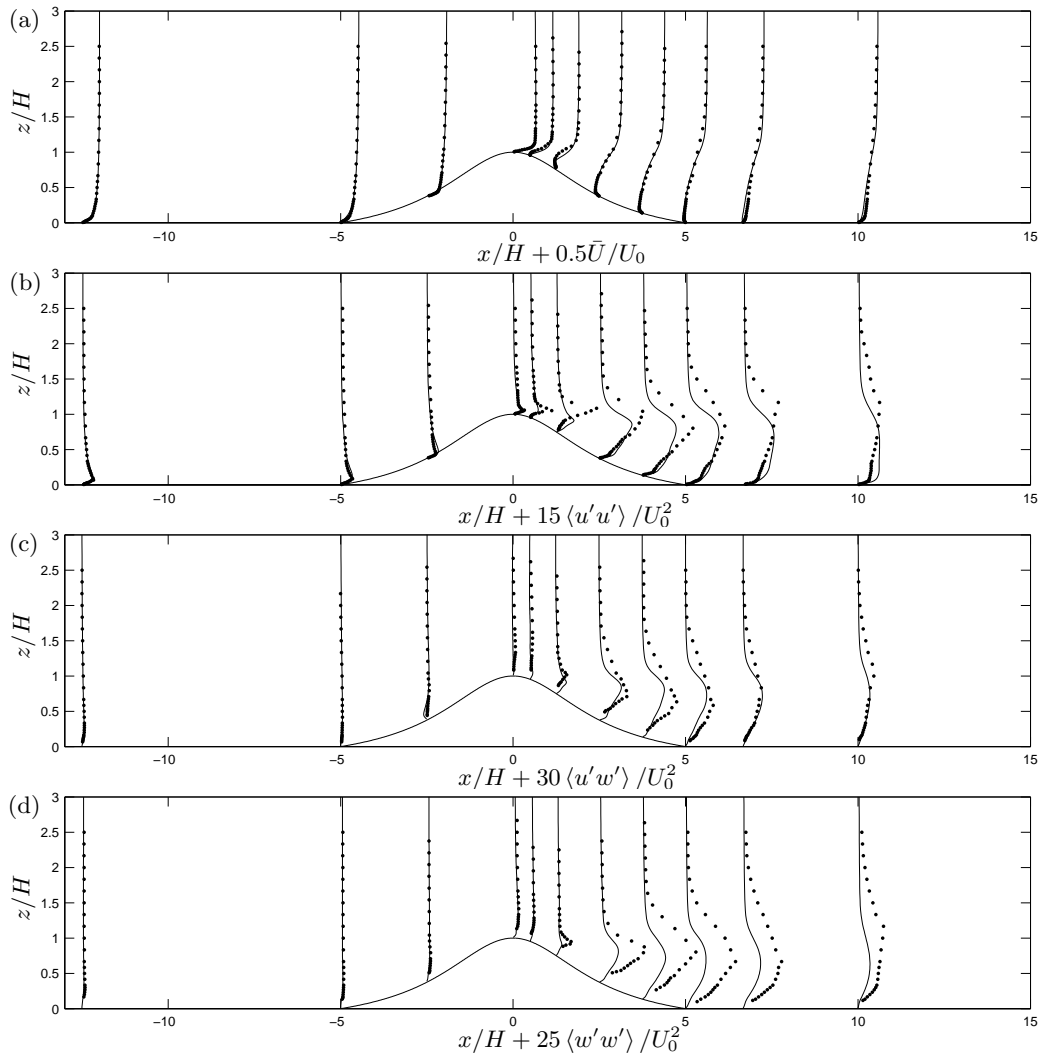


FIGURE 2. Comparison of ASBM closure simulation results for (a) mean streamwise velocity, Reynolds stress components (b) $\langle u'u' \rangle$, (c) $\langle u'w' \rangle$, and (d) $\langle w'w' \rangle$ with experimental results from Loureiro *et al.* (2007)

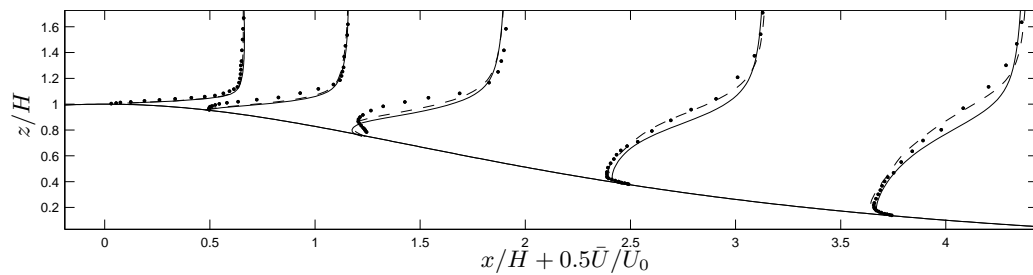


FIGURE 3. Comparison of streamwise velocity for simulation results of ASBM closure (- -), v^2f closure (—), and experimental results from Loureiro *et al.* (2007)

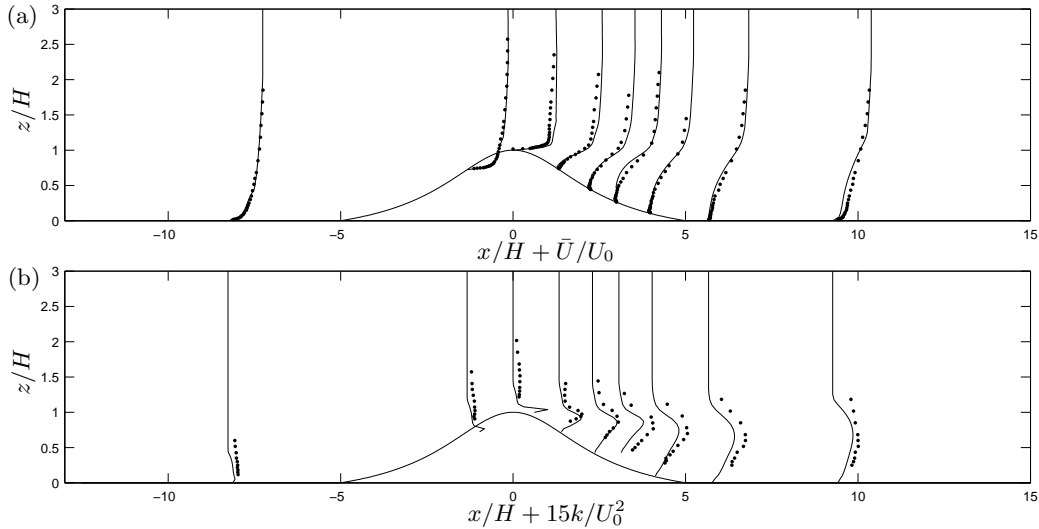


FIGURE 4. Comparison of v^2f closure simulation results for (a) mean streamwise velocity and (b) turbulent kinetic energy k with experimental results from Loureiro *et al.* (2009)

with a Reynolds number of 4,772 the requirements for the wall functions would mean a grid too coarse to capture any details of the flow. In their research, Loureiro *et al.* (2009) carried out experiments on the same geometry as their previous work but at higher Reynolds numbers so that the effects of wall roughness could be investigated. Accordingly, the high Reynolds number simulations were run with the same parameters so that comparisons could be made with their experimental data. Once again the boundary layer thickness at the inflow was 100mm but the Reynolds number was increased to 31,023. Also, the roughness length was set to 0.33mm. Figure 4 shows the results for the v^2f closure using a coarse grid and a rough wall function at the ground boundary. It can be seen that the agreement for the streamwise velocity is excellent. This size and height of the separated region is estimated accurately as is the reattachment point. Only a slight over-estimation of the speed up at the top of the ridge and slight under-estimation of the velocity recovery after reattachment can be seen. For the turbulent kinetic energy, the qualitative agreement is also good. In particular, both its form and magnitude are estimated well in the separated region and downstream. Upstream of the ridge and at its top, the agreement is less satisfactory. This may be because the Reynolds stress components, from which the turbulent kinetic energy is derived, are difficult to measure experimentally close to the ground. Thus the high values found estimated by the simulations are not apparent. Also, it is possible that the agreement in the upstream turbulent kinetic energy between the experiment and the inflow boundary conditions for the simulation was not sufficiently high.

5. Conclusions

A new coupling method was implemented for the algebraic structure-based turbulence model (ASBM) in both the unstructured-grid solver CDP and the open source CFD solver OpenFOAM. Both the ASBM and the v^2f turbulence closures were used to calculate the flow over a representative ridge, and the results were compared with previously published experimental data. Both closures demonstrate a good ability to predict the flow

including the characteristics of the separated region. The ASBM closure also captures the qualitative properties of the Reynolds stress components and accurately represents their relative magnitudes. New wall functions were developed for the v^2f closure and implemented in CDP. Simulations were carried out using the wall functions that include surface roughness, and comparisons were made with previously published experimental results. The wall functions are able to capture the important characteristics of the flow and reproduce the effects of the roughness while significantly reducing the grid resolution requirement. The successful application of the ASBM and v^2f closures in simulations of representative flows, along with the development of rough wall functions for the v^2f closure, show that there is significant potential for their use in modelling wind flow over complex terrain. Development of wall functions for the ASBM closure and the extension of the simulations to three dimensions will be part of ongoing research.

Acknowledgements

Many thanks go to Dr Juliana Loureiro for her help in providing the invaluable experimental data for comparison. JPO gratefully acknowledges support from the Center for Turbulence Research at Stanford University, the Todd Foundation, the Energy Education Trust of New Zealand, and the University of Auckland.

REFERENCES

- BOWEN, A. J. & MORTENSEN, N. G. 1996 Exploring the limits of WAsP: the wind atlas analysis and application program. In *European Wind Energy Conference and Exhibition*, pp. 584–587. Goeteborg, Sweden.
- EIDSVIK, K. J. 2005 A system for wind power estimation in mountainous terrain. prediction of Askervein hill data. *Wind Energy* **8** (2), 237–249.
- HANJALIC, K. 2005 Will RANS survive LES? a view of perspectives. *J. of Fluids Engineering* **127** (5), 831–839.
- HARGREAVES, D. M. & WRIGHT, N. G. 2007 On the use of the $k - \epsilon$ model in commercial CFD software to model the neutral atmospheric boundary layer. *J. of Wind Engineering and Industrial Aerodynamics* **95** (5), 355–369.
- KALITZIN, G., IACCARINO, G., LANGER, C. & KASSINOS, S. 2004 Combining eddy-viscosity models and the algebraic structure-based reynolds stress closure. In *Proceedings of the Summer Program*, pp. 171–182. Stanford.
- KASSINOS, S. & REYNOLDS, W. 1994 A structure-based model for the rapid distortion of homogeneous turbulence. *Tech. Rep.* TF-61. Mechanical Engineering Department, Stanford University.
- LANDBERG, L., MYLLERUP, L., RATHMANN, O., PETERSEN, E. L., JØRGENSEN, B. H., BADGER, J. & MORTENSEN, N. G. 2003 Wind resource estimation- an overview. *Wind Energy* **6** (3), 261–271.
- LAUNDER, B. E. & SPALDING, D. B. 1974 The numerical computation of turbulent flows. *Computer Methods in Applied Mechanics and Engineering* **3** (2), 269–289.
- LOUREIRO, J., MONTEIRO, A., PINHO, F. & SILVA FREIRE, A. 2009 The effect of roughness on separating flow over two-dimensional hills. *Experiments in Fluids* **46** (4), 577–596.
- LOUREIRO, J., PINHO, F. & SILVA FREIRE, A. 2007 Near wall characterization of the flow over a two-dimensional steep smooth hill. *Experiments in Fluids* **42** (3), 441–457.

- LOUREIRO, J. & SILVA FREIRE, A. 2009 Note on a parametric relation for separating flow over a rough hill. *Boundary-Layer Meteorology* **131** (2), 309–318.
- MORTENSEN, N. G., BOWEN, A. J. & ANTONIOU, I. 2006 Improving WASP predictions in (too) complex terrain. In *European Wind Energy Conference and Exhibition*. Athens, Greece.
- PALMA, J. M. L. M., CASTRO, F. A., RIBEIRO, L. F., RODRIGUES, A. H. & PINTO, A. P. 2008 Linear and nonlinear models in wind resource assessment and wind turbine micro-siting in complex terrain. *J. of Wind Engineering and Industrial Aerodynamics* **96** (12), 2308–2326.
- PERIVOLARIS, Y. G., VOUGIOUKA, A. N., ALAFOUZOS, V. V., MOURIKIS, D. G., ZAGORAKIS, V. P., RADOS, K. G., BARKOUTA, D. S., ZERVOS, A. & WANG, Q. 2006 Coupling of a mesoscale atmospheric prediction system with a CFD microclimatic model for production forecasting of wind farms in complex terrain: Test case in the island of Evia. In *European Wind Energy Conference and Exhibition*. Athens, Greece.
- POPE, S. B. 2000 *Turbulent flows*. Cambridge University Press, New York.
- RADHAKRISHNAN, H., PECNIK, R., IACCARINO, G. & KASSINOS, S. C. 2008 Computation of separated turbulent flows using the asbm model. In *Proceedings of the Summer Program 2008*, pp. 365–376. Stanford University.
- UNDHEIM, O., ANDERSSON, H. & BERGE, E. 2006 Non-linear, microscale modelling of the flow over Askervein Hill. *Boundary-Layer Meteorology* **120** (3), 477–495.
- WILCOX, D. C. 1998 *Turbulence modeling for CFD*, 2nd edn. DWC Industries, La Canada.
- WOOD, N. 2000 Wind flow over complex terrain: A historical perspective and the prospect for large-eddy modelling. *Boundary-Layer Meteorology* **96** (1), 11–32.